Supporting Information for

Molecular Motor Dnm1 Synergistically Induces Membrane Curvature To Facilitate Mitochondrial Fission

Michelle W. Lee,[†] Ernest Y. Lee,[†] Ghee Hwee Lai,[†,‡] Nolan W. Kennedy,[§] Ammon E. Posey,[‖] Wujing Xian,[†] Andrew L. Ferguson,[⊥,#] R. Blake Hill,[*,§] and Gerard C. L. Wong[*,†,¶,⊗]

[†]Department of Bioengineering, [¶]Department of Chemistry & Biochemistry, [⊗]California NanoSystems Institute, University of California, Los Angeles, Los Angeles, California 90095, United States

[‡]Present Address: Singapore Centre for Environmental Life Sciences Engineering (SCELSE), Singapore

[⊥]Department of Materials Science and Engineering, [#]Department of Chemical and Biomolecular Engineering University of Illinois at Urbana–Champaign, Urbana, IL 61801, United States

[§]Department of Biochemistry, Medical College of Wisconsin, Milwaukee, Wisconsin 53226, United States

[‖]Department of Biomedical Engineering, Washington University in St. Louis, St. Louis, Missouri 63130, United States

Corresponding authors

*E-mail: gclwong@seas.ucla.edu or rbhill@mcw.edu

File Contents

Supplementary Figure S5. Multiple sequence alignment of dynamin superfamily proteins

Supplementary Table S1. Machine-learning screen and phylogenetic distances of dynamins

Dnm1 and Fis1 expression and purification

A pMALc2x plasmid encoding the gene for *E. coli* maltose-binding protein (MBP), followed by ENLYFQS (a tobacco etch virus (TEV) protease recognition sequence) and the *S. cerevisiae* Dnm1 sequence, was transformed into Rosetta cells (Novagen) and grown at 37 ºC to an OD600 of 0.5 in Super Broth with chloramphenicol (34 μg/mL) and kanamycin (30 μg/mL). Protein expression was induced with 0.6 mM isopropyl 1-thio-β-D-galactopyranoside at 18 ºC overnight. Cells were harvested by centrifugation and resuspended in MBP column buffer (50 mM phosphate pH 7.4, 500 mM NaCl, 5 mM $MgCl_2$, 1 mM DTT) containing protease inhibitors (Roche Applied Science). Cells were lysed with 5 passes through an EmulsiFlex C3 (Avestin) at 20,000 psi. DNase was added to the lysate to 2 μg/mL, and cell debris was removed by centrifugation. The resulting supernatant was applied to an amylose resin (New England BioLabs) and the desired product eluted using 20 mM maltose added to MBP buffer. The MBP-tag was cleaved by incubation with TEV protease (1:100 molar ratio) overnight at 4 °C and the reaction mixture was applied to an S200 size exclusion column to separate MBP from Dnm1. The mass of Dnm1 was confirmed by mass spectrometry and the purity was evaluated to be >90% homogeneous by Coomassie-stained SDS-PAGE.

For Fis1, protein was expressed and purified as previously described.[1] A pET29b plasmid encoding the *S. cerevisiae* Fis1 gene lacking the last 27 amino acids, followed by the amino acid sequence ENLYFQS that is recognized by TEV protease and a 6xHis tag, was transformed into Rosetta cells (Novagen) and grown at 37 ºC to an OD600 of 0.6–0.9 in Luria Broth with chloramphenicol (34 μg/mL) and kanamycin (30 μg/mL). Protein expression was induced with 0.4 mM isopropyl 1-thio-β-D-galactopyranoside at 18 ºC overnight. Cells were harvested by centrifugation and resuspended in column buffer A (25 mM Tris pH 7.4, 50 mM NaCl and 30 mM imidazole) containing protease inhibitors (Roche Applied Science). Cells were lysed by three passes through an Emulsiflex C3 Homogenizer (Avestin) at 20,000 psi. DNase was added at 1 μg/mL with 10 mM $MgCl_2$, and the lysates were clarified by centrifugation. Fis1-His was isolated by Ni^{2+} affinity chromatography (GE-Amersham) and eluted in column buffer containing 500 mM imidazole. TEV protease was added to pooled fractions from the elution at 1:100 molar ratio for 4 hours at room temperature to cleave the C-terminal 6xHis tag. The resulting reaction mixture was re-applied to Ni^{2+} affinity resin re-equilibrated in column buffer A. Fis1 from the flow-through was collected, concentrated, and applied to an SE-75 sizing column (GE-Amersham). Sample purity was assessed by Coomassie-stained SDS-PAGE and found to be >95% pure. Mass was confirmed by MALDI-TOF mass spectrometry.

Machine-learning screen for membrane-active sequences

Full details of the membrane activity prediction tool are described in prior work.[2] Here, we employ the classifier to identify putative membrane-active subsequences within proteins Dnm1/Drp1 and Fis1. Using Python, all subsequences of 10–25 amino acids in length were generated for these two proteins and cross-referenced with either the known secondary structure

from crystallographic data or from a secondary structure prediction algorithm. Helical segments from Dnm1/Drp1 and Fis1 were screened using the machine-learning classifier, and σ and $P(+1)$ values were sorted and tabulated. The top helical subsequences for each protein were sorted by $P(+1)$. In other analyses, sequences from 33 dynamin superfamily members that aligned with the top helical segments of Dnm1/Drp1 were screened in a similar manner.

To generate a probability map for segments of Dnm1 that contain a high probability for membrane activity, all subsequences were aligned with the entire Dnm1 sequence. A normalized net σ score was assigned to each residue, equal to the sum of all σ scores corresponding to subsequences in which that residue appears, divided by the number of times that amino acid appears in a subsequence (Figure 1A). This ensures that residues are weighted by the magnitude of σ, which is proportional to the likelihood of membrane activity.

Sequence alignment and 3D modeling

Initial sequence alignment of Dnm1 and Drp1 was carried out using T-Coffee (http://tcoffee.crg.cat/apps/tcoffee/index.html), and the outputs were formatted using BoxShade (http://www.ch.embnet.org/software/BOX_form.html). Homology model of Dnm1 was generated from Drp1 using MODELLER.[3] All 3D images for Dnm1, Drp1, Fis1, and hFis1 were generated with MODELLER or the Tachyon plugin for VMD.

SAXS experiments

Lyophilized phospholipids 1,2-dioleoyl-*sn*-glycero-3-phosphoethanolamine (DOPE), 1,2-dioleoyl-*sn*-glycero-3-phosphocholine (DOPC), and cardiolipin (CL) were obtained from Avanti Polar Lipids and dissolved in chloroform at 20 mg/mL to produce individual lipid stock solutions. Ternary lipid compositions were prepared from the lipid stock solutions as mixtures of DOPE/DOPC/CL at molar ratios of 75/15/10 and 75/5/20, evaporated under nitrogen, and desiccated under vacuum overnight to form a dry lipid film. Lipid films were resuspended in aqueous 100 mM KCl, 10 mM *N*-(2-hydroxyethyl)piperazine-*N*'-ethanesulfonic acid (HEPES) (pH 7.4) to a concentration of 20 mg/mL. Lipid suspensions were incubated overnight at 37 °C, sonicated until clear, and extruded through a 0.2 μm pore Nucleopore filter (Whatman) to form SUVs.

The Dnm1 and Fis1 protein concentrations used in SAXS experiments were comparable to those used in a large number of protein–lipid interaction studies for Dnm1 and Fis1.[4-10] Solubilized Dnm1 and Fis1 were mixed with SUVs at specified P/L molar ratios and hermetically sealed into quartz capillaries (Hilgenberg GmbH, Mark-tubes) for SAXS measurements taken at the Stanford Synchrotron Radiation Lightsource (SSRL, beamline 4-2) using monochromatic X-rays with an energy of 9 keV. A Rayonix MX255-HE detector (73.2 μm pixel size) was used to collect the scattered radiation and the resulting 2D SAXS powder patterns were integrated using Nika 1.50[11] package for Igor Pro 6.31 and FIT2D.[12]

For experiments with MBP-Dnm1, SUVs were prepared from a third ternary lipid composition of DOPE/DOPC/1,2-dioleoyl-*sn*-glycero-3-phospho-L-serine (DOPS) at a molar ratio of 75/5/20. SUVs were incubated with MBP-Dnm1 (P/L = 1/1300) alone or in combination

with Fis1 (P/L = 1/650) and their resulting membrane structures were characterized using SAXS as described above.

SAXS data were analyzed by plotting the integrated scattering intensity $I(Q)$ against Q using Origin Lab software. The phases present in each sample were determined by comparing the ratios of measured peak positions, $Q_{measured}$, with those of the permitted reflections for different crystal phases. The linear regression through points corresponding to the peaks was then used to calculate the lattice parameter, a, of each identified phase. For both powder-averaged hexagonal and cubic phases, each peak was represented by a point having coordinates of the assigned reflection, in terms of Miller indices (h, k, l), and $Q_{measured}$. For a hexagonal phase, $Q = \left(4\pi/\left(a\sqrt{3}\right)\right)\sqrt{h^2 + hk + k^2}$, and for a cubic phase, $Q = (2\pi/a)\sqrt{h^2 + k^2 + l^2}$, where a is the lattice parameter. The slopes of the regressions of $Q_{measured}$ versus $\sqrt{h^2 + hk + k^2}$ and $Q_{measured}$ versus $\sqrt{h^2 + k^2 + l^2}$ are $4\pi/\left(a\sqrt{3}\right)$ and $2\pi/a$, respectively, which can then be used to calculate a.

Phylogenetic analysis

A multiple sequence alignment of 33 dynamin superfamily members was carried out with default parameters using MUSCLE.[13,14] Newick tree topologies were extracted from the multiple sequence alignment using Simple Phylogeny (http://www.ebi.ac.uk/Tools/phylogeny/simple_phylogeny/). A phylogram was reconstructed using TreeVector.[15]

Statistical analysis

Bootstrap analysis for linear and nonlinear correlations were done in R. Correlation coefficients, 95% confidence intervals, and P-values were calculated with N = 100,000 sampling iterations. The 'minerva'[16] and 'energy'[17] packages were used to calculate MIC and dCor respectively. Null-hypothesis significance tests were carried out with a significance threshold α = 0.05.

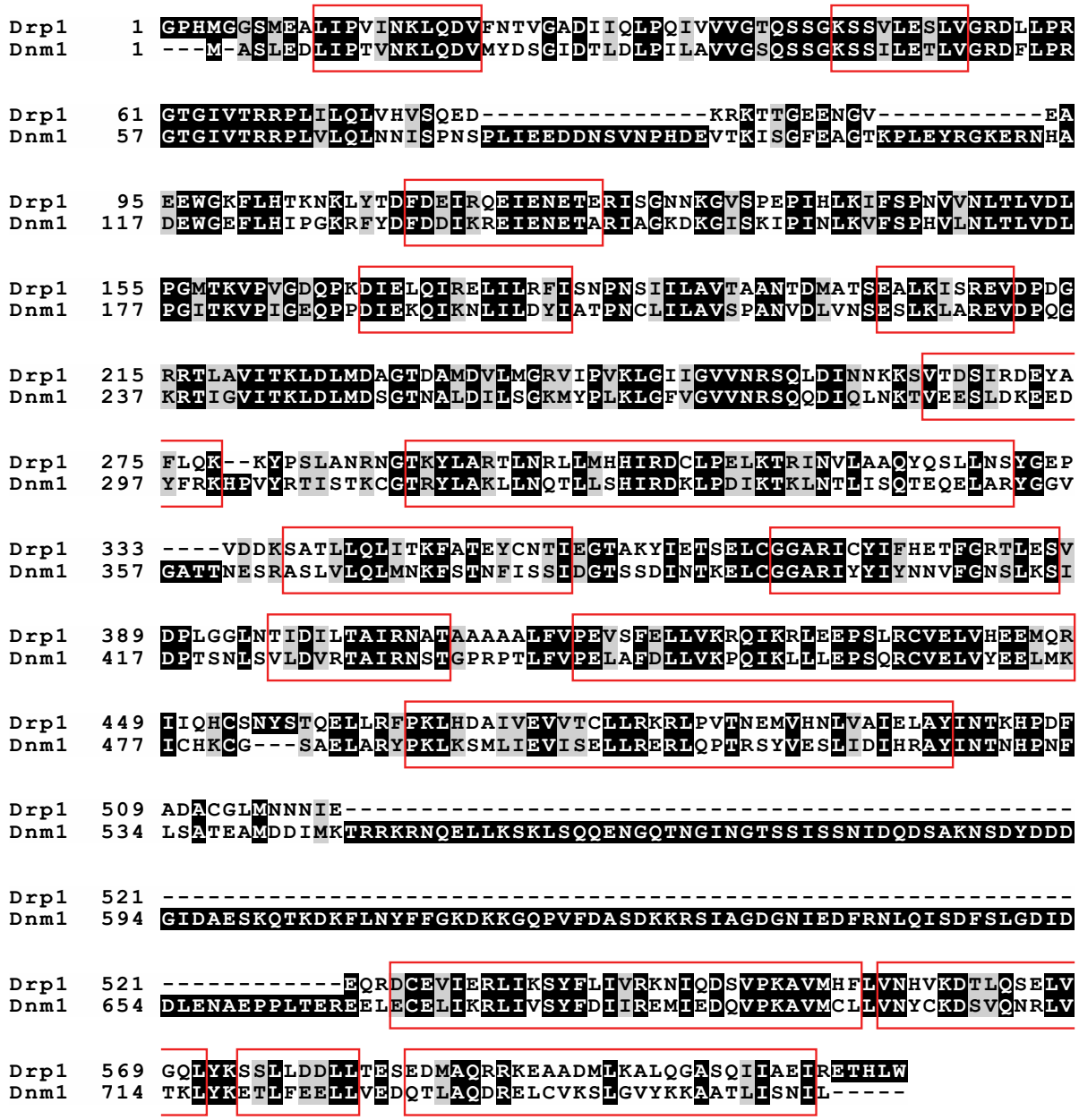

Figure S1. Full sequence alignment of Drp1 and Dnm1. Putative helical domains are boxed in red.

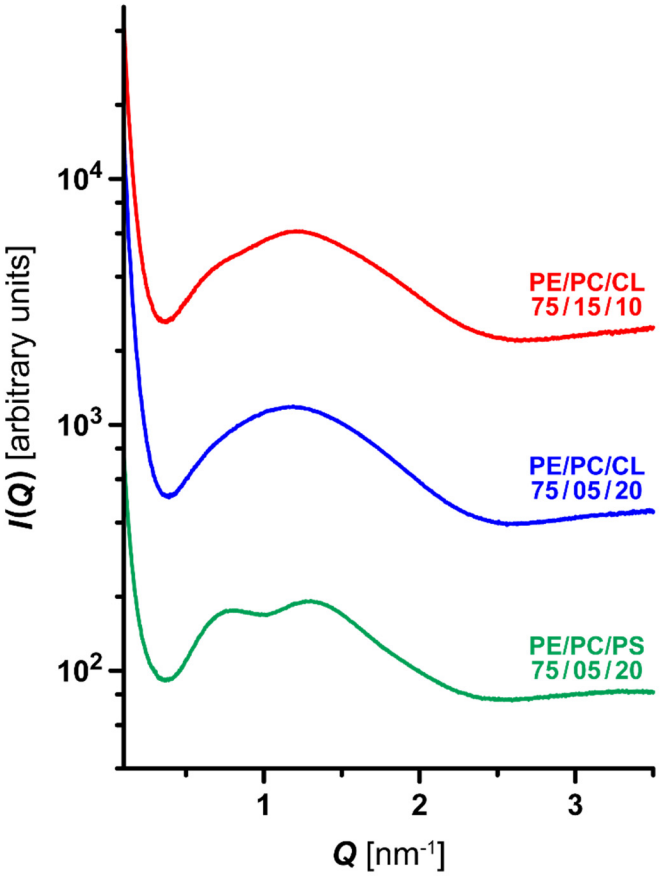

Figure S2. SAXS spectra for SUV control samples. 75/15/10 and 75/5/20 PE/PC/CL, and 75/5/20 PE/PC/PS lipid vesicles displayed form factors consistent with that of unilamellar vesicles.

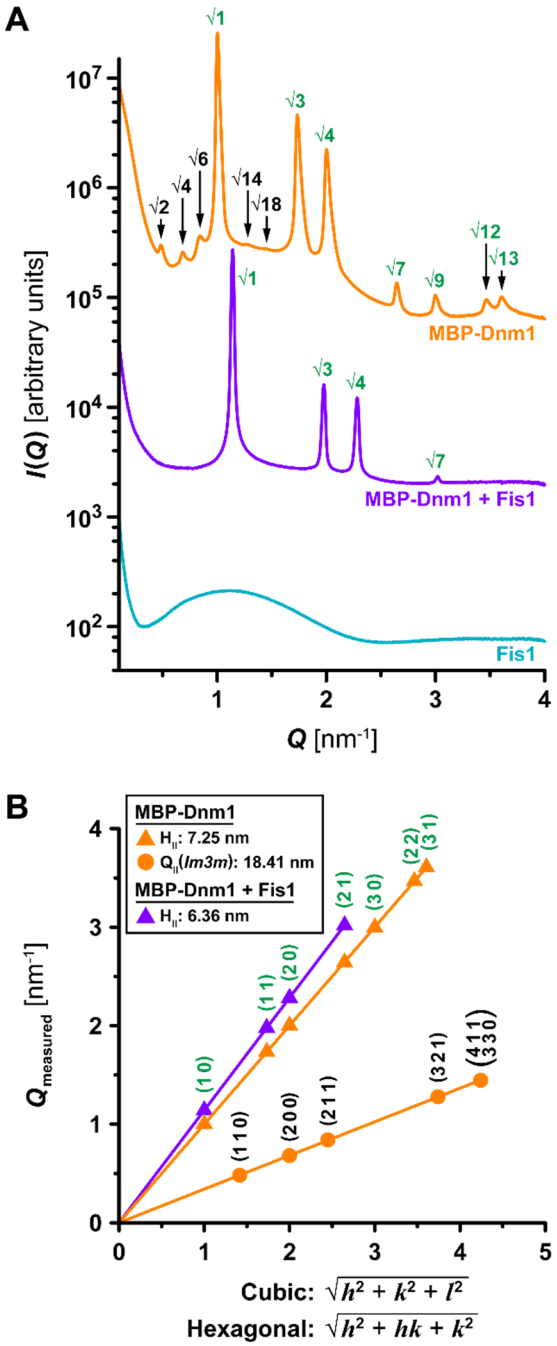

Figure S3. SAXS spectra for SUVs with MBP-Dnm1 alone and in the presence of Fis1. (A) MBP-Dnm1 (*P*/*L* = 1/1300) incubated with 75/5/20 PE/PC/PS model membrane resulted in H_{II} and *Im3m* Q_{II} phases (top curve). Correlation peaks corresponding to assigned reflections are indicated for hexagonal (green) and cubic (black) phases. Like with the PE/PC/CL membranes, Fis1 (*P*/*L* = 1/650) also did not restructure the 75/5/20 PE/PC/PS membrane (bottom curve). When MBP-Dnm1 and Fis1 are incubated together with 75/5/20 PE/PC/PS SUVs, the *Im3m* Q_{II} phase that was induced by MBP-Dnm1 alone is no longer present (middle curve). **(B)** Indexing of H_{II} and *Im3m* Q_{II} phases generated in the 75/5/20 PE/PC/PS membrane and their respective lattice parameters.

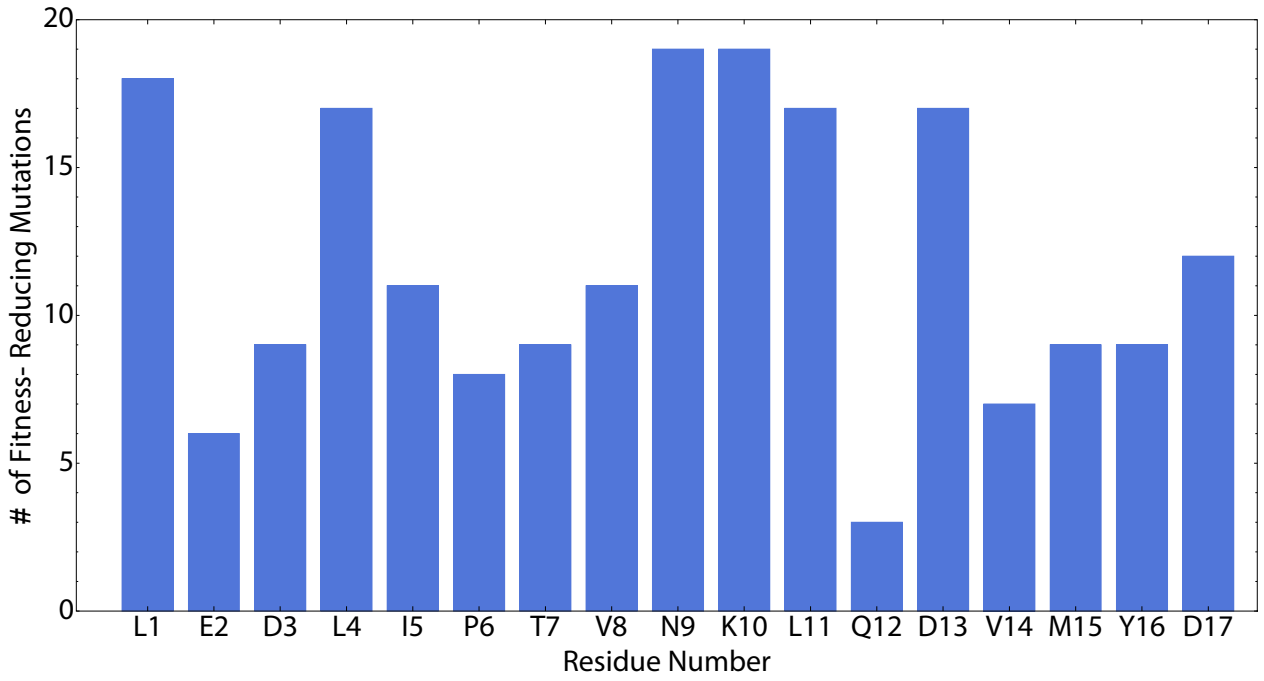

Figure S4. Mutability analysis of the Dnm1 N-terminal helix. Plot of the total number of fitness-reducing single mutations ($\Delta\sigma < 0$) at each amino acid along the length of the N-terminal helix of Dnm1. 19 total mutations are possible at each of the 17 positions. Residues L1, L4, N9, K10, L11, D13, and D17 exhibit strong aversion to mutation. A 2D heat map and distribution of all single mutants of this helix are found in Figure 6A,B.

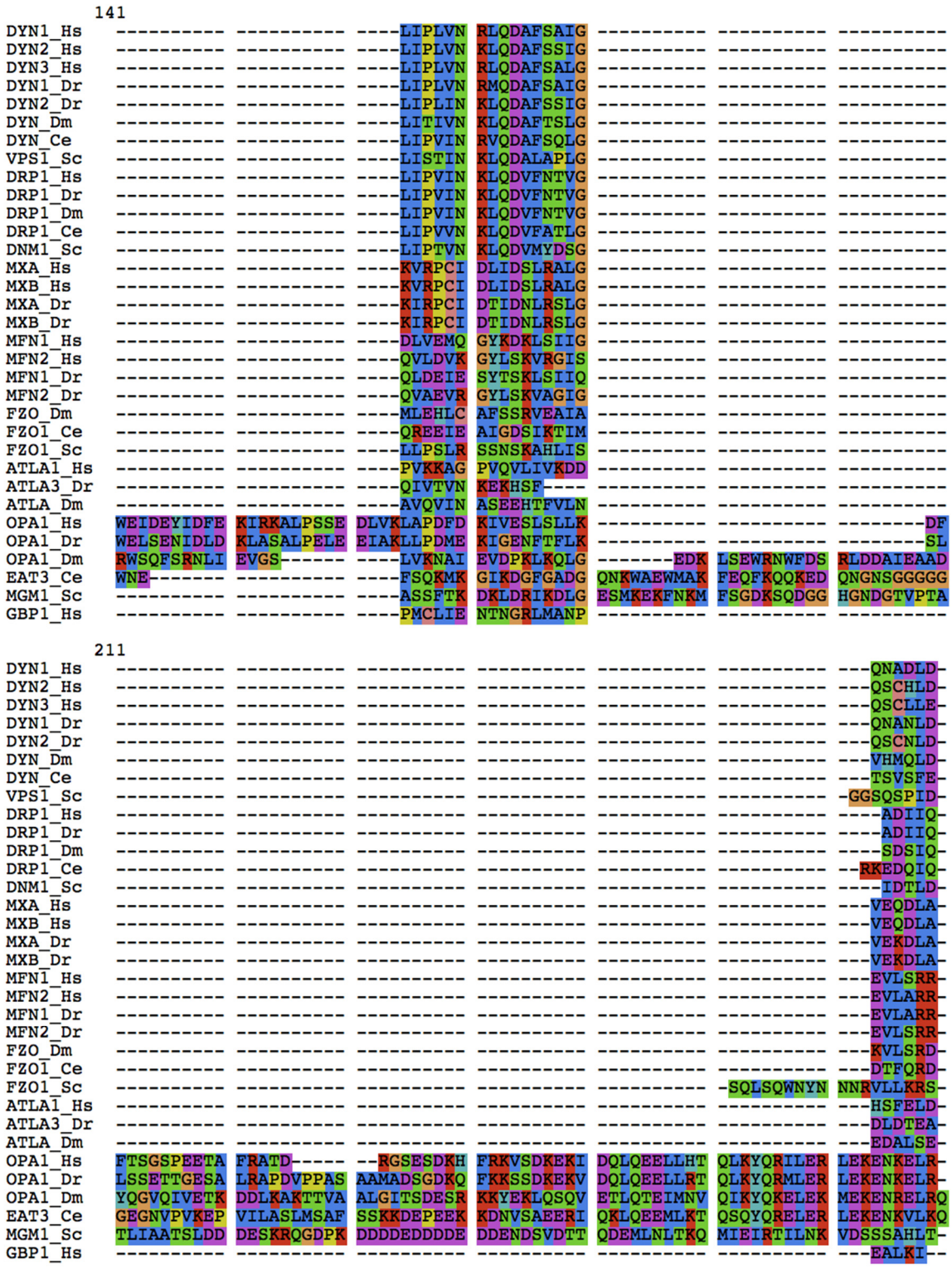

Figure S5. Multiple sequence alignment of dynamin superfamily proteins. Multiple sequence alignment of Dnm1/Drp1 with other dynamin superfamily members shows the conserved helix in N-terminal region (top half).

Table S1. Machine-learning screen and phylogenetic distances of dynamins. 33 dynamin family members were screened for membrane activity using the previously described machine-learning algorithm. Membrane activity prediction (+1 or −1), distance-to-hyperplane (σ), probability of classification ($P(+1)$), aligned sequence, phylogenetic distance, and accession codes are reported for each sequence. This data is plotted in Figure 6D.

ID	Prediction	σ	$P(+1)$	Sequence	Phylogenetic Distance	Uniprot Accession Codes
DYN1_Hs	1	0.69	0.91	LIPLVNRLQDA FSAIG	0.00	sp|Q05193|DYN1_HUMAN
DYN2_Hs	1	2.60	1.00	LIPLVNKLQDA FSSIG	0.33	sp|P50570|DYN2_HUMAN
DYN3_Hs	1	0.71	0.91	LIPLVNRLQDA FSALG	0.32	sp|Q9UQ16|Dynamin-3
DYN1_Dr	1	0.03	0.53	LIPLVNRMQDA FSAIG	0.15	tr|E4VNZ2|E4VNZ2_DANRE
DYN2_Dr	1	2.68	1.00	LIPLINKLQDAF SSIG	0.31	tr|Q4V8Z7|Q4V8Z7_DANRE
DYN_Dm	1	2.35	1.00	LITIVNKLQDA FTSLG	0.61	sp|P27619|Dynamin
DYN_Ce	1	0.78	0.93	LIPVINRVQDA FSQLG	0.72	sp|P39055|DYN1_CAEEL
VPS1_Sc	1	2.14	1.00	LISTINKLQDAL APLG	2.18	sp|P21576|Vacuolar
DRP1_Hs	1	2.41	1.00	LIPVINKLQDV FNTVG	2.23	sp|O00429|DNM1L_HUMAN
DRP1_Dr	1	2.41	1.00	LIPVINKLQDV FNTVG	2.23	sp|Q7SXN5|DNM1L_DANRE
DRP1_Dm	1	2.41	1.00	LIPVINKLQDV FNTVG	2.27	tr|Q9VQE0|Q9VQE0_DROM E
DRP1_Ce	1	1.96	1.00	LIPVVNKLQDV FATLG	2.26	tr|G5EDY8|G5EDY8_CAEEL
DNM1_Sc	1	1.41	0.99	LIPTVNKLQDV MYDSG	2.25	sp|P54861|Dynamin-related
MXA_Hs	-1	-0.29	0.29	KVRPCIDLIDSL RALG	4.16	sp|P20591|MX1_HUMAN
MXB_Hs	-1	-0.29	0.29	KVRPCIDLIDSL RALG	4.38	sp|P20592|Interferon-induced
MXA_Dr	-1	-0.09	0.43	KIRPCIDTIDNL RSLG	4.00	sp|Q8JH68|Interferon-induced
MXB_Dr	-1	-0.09	0.43	KIRPCIDTIDNL RSLG	4.07	sp|Q800G8|Interferon-induced
MFN1_Hs	-1	-1.42	0.01	DLVEMQGYKD KLSIIG	7.93	sp|Q8IWA4|MFN1_HUMAN
MFN2_Hs	-1	-0.47	0.18	QVLDVKGYLS KVRGIS	8.09	sp|O95140|MFN2_HUMAN
MFN1_Dr	-1	-0.58	0.13	QLDEIESYTSK LSIIQ	7.71	tr|Q6PFP9|Q6PFP9_DANRE
MFN2_Dr	1	0.57	0.87	QVAEVRGYLS KVAGIG	8.05	tr|A8WIN6|A8WIN6_DANRE
FZO_Dm	-1	-0.70	0.09	MLEHLCAFSSR VEAIA	7.38	sp|O18412|Transmembrane

FZO1_Ce	-1	-1.59	0.01	QREEIEAIGDSIKTIM	8.28	sp|Q23424|Transmembrane
FZO1_Sc	-1	-0.03	0.49	LLPSLRSSNSKAHLIS	10.25	sp|P38297|Mitofusin
ATLA1_Hs	-1	-1.14	0.02	PVKKAGPVQVLIVKDD	8.49	sp|Q8WXF7|ATLA1_HUMAN
ATLA3_Dr	-1	-0.38	0.23	QIVTVNKEKHSFDLDT	8.59	tr|Q5XJ96|Q5XJ96_DANRE
ATLA_Dm	-1	-1.40	0.01	AVQVINASEEHTFVLN	8.49	sp|Q9VC57|Atlastin
OPA1_Hs	-1	-0.75	0.08	LAPDFDKIVESLSLLK	5.78	sp|O60313|OPA1_HUMAN
OPA1_Dr	-1	-0.74	0.08	LLPDMEKIGENFTFLK	5.73	sp|Q5U3A7|Dynamin-like
OPA1_Dm	-1	-2.36	0.00	LVKNAIEVDPKLKQLG	5.30	tr|A1Z9N0|A1Z9N0_DROME
EAT3_Ce	-1	-0.55	0.14	FSQKMKGIKDGFGADG	5.67	tr|Q18965|Q18965_CAEEL
MGM1_Sc	1	0.39	0.79	ASSFTKDKLDRIKDLG	4.58	sp|P32266|Dynamin-like
GBP1_Hs	-1	-1.17	0.02	PMCLIENTNGRLMANP	8.53	sp|P32455|GBP1_HUMAN

References

(1) Picton, L. K.; Casares, S.; Monahan, A. C.; Majumdar, A.; Hill, R. B. Evidence for Conformational Heterogeneity of Fission Protein Fis1 From Saccharomyces Cerevisiae. *Biochemistry* **2009**, *48*, 6598–6609.

(2) Lee, E. Y.; Fulan, B. M.; Wong, G. C. L.; Ferguson, A. L. Mapping Membrane Activity in Undiscovered Peptide Sequence Space Using Machine Learning. *Proc. Natl. Acad. Sci. U. S. A.* **2016**, *113*, 13588–13593.

(3) Webb, B.; Sali, A. Comparative Protein Structure Modeling Using MODELLER. *Curr. Protoc. Bioinform.* **2014**, *47*, 5.6.1–5.6.32.

(4) Lackner, L. L.; Horner, J. S.; Nunnari, J. Mechanistic Analysis of a Dynamin Effector. *Science* **2009**, *325*, 874–877.

(5) Mears, J. A.; Lackner, L. L.; Fang, S.; Ingerman, E.; Nunnari, J.; Hinshaw, J. E. Conformational Changes in Dnm1 Support a Contractile Mechanism for Mitochondrial Fission. *Nat. Struct. Mol. Biol.* **2011**, *18*, 20–26.

(6) Fröhlich, C.; Grabiger, S.; Schwefel, D.; Faelber, K.; Rosenbaum, E.; Mears, J.; Rocks, O.; Daumke, O. Structural Insights Into Oligomerization and Mitochondrial Remodelling of Dynamin 1-Like Protein. *EMBO J.* **2013**, *32*, 1280–1292.

(7) Ugarte-Uribe, B.; Müller, H.-M.; Otsuki, M.; Nickel, W.; García-Sáez, A. J. Dynamin-Related Protein 1 (Drp1) Promotes Structural Intermediates of Membrane Division. *J. Biol. Chem.* **2014**, *289*, 30645–30656.

(8) Koppenol-Raab, M.; Harwig, M. C.; Posey, A. E.; Egner, J. M.; MacKenzie, K. R.; Hill, R. B. A Targeted Mutation Identified Through pKa Measurements Indicates a Postrecruitment Role for Fis1 in Yeast Mitochondrial Fission. *J. Biol. Chem.* **2016**, *291*, 20329–20344.

(9) Chang, C.-R.; Manlandro, C. M.; Arnoult, D.; Stadler, J.; Posey, A. E.; Hill, R. B.; Blackstone, C. A Lethal De Novo Mutation in the Middle Domain of the Dynamin-Related GTPase Drp1 Impairs Higher Order Assembly and Mitochondrial Division. *J. Biol. Chem.* **2010**, *285*, 32494–32503.

(10) Francy, C. A.; Alvarez, F. J. D.; Zhou, L.; Ramachandran, R.; Mears, J. A. The Mechanoenzymatic Core of Dynamin-Related Protein 1 Comprises the Minimal Machinery Required for Membrane Constriction. *J. Biol. Chem.* **2015**, *290*, 11692–11703.

(11) Ilavsky, J. Nika: Software for Two-Dimensional Data Reduction. *J. Appl. Crystallogr.* **2012**, *45*, 324–328.

(12) Hammersley, A. P. FIT2D: an Introduction and Overview. *European Synchrotron Radiation Facility Internal Report: ESRF97HA02T* **1997**.

(13) Edgar, R. C. MUSCLE: Multiple Sequence Alignment with High Accuracy and High Throughput. *Nucleic Acids Res.* **2004**, *32*, 1792–1797.

(14) Edgar, R. C. MUSCLE: a Multiple Sequence Alignment Method with Reduced Time and Space Complexity. *BMC Bioinf.* **2004**, *5*, 113.

(15) Pethica, R.; Barker, G.; Kovacs, T.; Gough, J. TreeVector: Scalable, Interactive, Phylogenetic Trees for the Web. *PLoS ONE* **2010**, *5*, e8934.

(16) Albanese, D.; Filosi, M.; Visintainer, R.; Riccadonna, S.; Jurman, G.; Furlanello, C. Minerva and Minepy: a C Engine for the MINE Suite and Its R, Python and MATLAB Wrappers. *Bioinformatics* **2013**, *29*, 407–408.

(17) Székely, G. J.; Rizzo, M. L.; Bakirov, N. K. Measuring and Testing Dependence by Correlation of Distances. *Ann. Statist.* **2007**, *35*, 2769–2794.